Astron. Astrophys. 310, 211–220 (1996)

ASTRONOMY AND ASTROPHYSICS

Spectropolarimetry of symbiotic stars

On the binary orbit and the geometric structure of V 1016 Cygni*

H. Schild[1] **and H.M. Schmid**[2]

[1] Institut für Astronomie, ETH-Zentrum, CH-8092 Zürich, Switzerland
[2] Mount Stromlo and Siding Spring Observatories, ANU, Weston Creek P.O., ACT 2611, Canberra, Australia

Received 10 August 1995 / Accepted 19 October 1995

Abstract. We present spectropolarimetric observations of the symbiotic Mira V 1016 Cygni which cover the broad emission features at λ6825 and λ7082. The λ6825 line, which is due to Raman scattering of O VI λ1032 emission, strongly increased its degree of polarization over a period of 3 years. The polarization angle in the blue line wing is found to rotate clock-wise at a constant rate of 8 ± 2 °/yr. We interpret these changes as due to the binary motion. The binary axis, projected onto the celestial sphere was at a position angle of 81° in August 1991 and rotated to 58° in September 1994. The polarization changes in the λ6825 Raman line also indicate, that the V 1016 Cyg system was close to conjunction in August 1991 and that the orbit inclination is $60° \pm 20°$. The binary period is most likely in the range of 80 ± 25 yrs.

We find that the line of nodes of the orbital plane of V 1016 Cyg has roughly a North-South orientation. This is in agreement with the bipolar outflow model proposed by Solf (1983) from emission line observations.

The observed polarization structure in the Raman scattered O VI lines is not compatible with a scattering geometry which is rotationally symmetric around the binary axis. We adopt a 3-dimensional scattering model for the innermost region of the binary system. It consists of a Mira variable with a radially symmetric neutral wind region which is terminated on the hot components side by an ionization front which is warped due to the relative binary and wind motions.

We identify in the spectrum of V 1016 Cyg further Raman features: The broad emission bumps at $\lambda\lambda$7023,7054 are due to Raman scattering of C II λ1036,1037 at neutral hydrogen.

Key words: binaries: symbiotic – individual stars: V 1016 Cygni – polarization – scattering

1. Introduction

Symbiotic Miras form binaries together with a hot white dwarf as a companion. Although they are very wide systems they show various interaction phenomena, like nova-like outbursts or strong irradiation effects. Extended and sometimes asymmetric nebular structures, which may well be another manifestation of the interaction, have been mapped around many of these objects. The best known examples are R Aqr (Solf & Ulrich 1985; Paresce & Hack 1994), He2-104 (Schwarz et al. 1989; Corradi & Schwarz 1993) or HM Sge (e.g. Hack & Paresce 1993; Eyres et al. 1995).

Interaction and mass outflow phenomena in symbiotic systems have also been studied theoretically (e.g. Girard & Willson 1987; Nussbaumer & Walder 1993), but most of these investigations and the interpretation of the observational data suffer from a pressing lack of knowledge on basic orbital parameters. It is therefore difficult to verify any model for the mass outflow and the formation of extended nebular structures. Up to now there exists no observational evidence, as to whether the extended structures in symbiotic Miras are due to polar, meridional, or equatorial outflows.

It is presently thought that the periods of symbiotic Miras lie in the range 20 – 200 years (Whitelock 1987) but no reliable measurements are available. Several attempts have been made to determine the period of R Aqr, the brightest system of this class. Willson et al. (1981) have suggested that obscurations of the Mira at various epochs may be due to eclipses by a dust cloud associated with the hot companion thereby inferring a binary period of 44 years. Wallerstein (1986) made an attempt to derive a radial velocity curve from absorption features of the Mira in the system. His data are consistent with such an orbital period, but, as stated by the author himself, his results would make a good candidate "in a contest for the least certain orbit of a spectroscopic binary". Radial velocity variations of the nebular emission lines have also been measured (Merrill 1950, Anandarao et al. 1985), however, it is unclear whether there is a close link between such variations and the orbital motion.

Send offprint requests to: H. Schild

* Based on observations obtained with the William Herschel Telescope of the Royal Greenwich Observatory, La Palma, Canary Islands

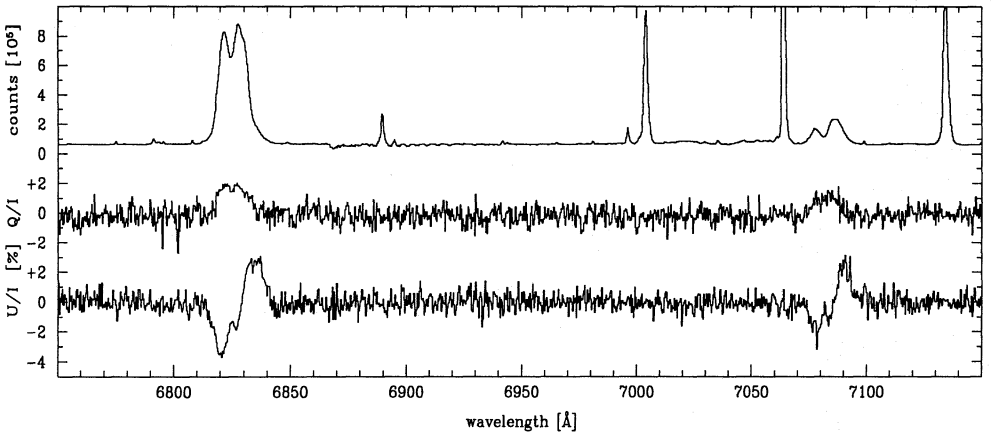

Fig. 1. Total flux (top) and relative Stokes parameters of V 1016 Cyg as observed in Sep 1994. Polarization signals are only detected in the two Raman scattered lines at λ6825 and λ7082.

Equally unconvincing were attempts made for the symbiotic Mira V 1016 Cyg. Wallerstein et al. (1984) conclude from emission line profile variations that the orbital period is probably at least several decades. This is a reasonable result considering the expected Roche geometry of a detached Mira + white dwarf binary system. More questionable in this respect is the short orbital period (P = 9.5 years) suggested by Nussbaumer & Schmid (1988) based on UV line flux variations; indeed, subsequent (unpublished) observations do not follow the predicted light curve. An even shorter period of 6 years was suggested by Munari (1988) from IR colours collected from the literature. We reanalyzed these data and found that there exist large discrepancies between different observers in both, colour calibration and temporal variability. This makes the suggested 6 year periodicity highly uncertain.

In this paper we illustrate how spectropolarimetric observations of the broad emission lines at λ6825 and λ7082 can be used to derive information about the orbit and the geometric structure of a symbiotic Mira. These emission lines are produced by a Raman scattering process of the O VI $\lambda\lambda$1032,1038 resonance lines by neutral hydrogen (Schmid 1989). In symbiotic systems strong O VI line radiation is produced in the ionized region near the hot component and converted by neutral hydrogen in the extended atmosphere of the cool giant into $\lambda\lambda$6825,7082 photons. Raman scattering is a dipole process and therefore produces observable light polarization for an anisotropic scattering geometry. Spectropolarimetric observations have shown that the O VI Raman lines are indeed polarized (Schmid & Schild 1990, 1994).

The expectation that the polarization signal in the Raman scattered lines changes as a result of the orbital motion is the key for determining the orbital periods. Even in the case of binaries with very long orbital periods, the rotation of the polarization angle is measurable after a relatively short time interval, which may cover only a fraction of the total period. Thus, first estimates of the periods of symbiotic Miras can be obtained within the time horizon of a current research grant.

The observation of phase locked scattering polarization provides not only the binary period but also information about the orientation and inclination of the orbital plane. This is particularly useful for the V 1016 Cyg system, because spatial structures on the subarcsec scale have been detected with optical and radio telescopes (Hjellming & Bignell 1982; Solf 1983; Taylor 1988). The orientation of the orbital plane with respect to the extended nebular structure will help the interpretation of mass outflow mechanisms and wind interactions in symbiotic systems. Additionally, we can extract geometric and dynamic information about the innermost region of symbiotic binaries. This is possible because the polarization angle of the scattered light traces the direction of the incoming light while the spectral dependence can be associated with Doppler shifts introduced in the scattering process.

Here we present first results for the symbiotic Mira V 1016 Cyg from an ongoing spectropolarimetric monitoring program of northern symbiotic systems. Section 2 describes the observations and Sect. 3 presents the data followed by an analysis of the polarization variations in Sect. 4. In Sect. 5 we present a simple model for the geometric structure of V 1016 Cyg and compare it to existing observations. We discuss our findings in Sect. 7. As a spin-off from our observations we report in Sect. 6 the detection of previously unrecognized Raman scattered emission lines at λ7023 and λ7054, which are due to scattering of C II $\lambda\lambda$1036,1037 by neutral hydrogen.

2. Observations

Spectropolarimetric observations of V 1016 Cyg were obtained with the 4.2m telescope (WHT) of the Royal Greenwich Observatory on La Palma, Canary Islands. The data were collected in service mode with the ISIS spectrograph during the nights of 18 August 1991, 17 September 1992, 5 October 1992, 27 Mai 1993 and 18 September 1994. The first of these observation was taken with the 600R grating and suffered from a considerably degraded spectral resolution because of a focusing error (Schmid & Schild 1994 henceforth referred to as Paper I). The other observations were obtained with the 1200R grating which provided a resolution of 0.65 Å. The detector was a coated EEV CCD with 1242×1152 pixels, each 22.5 μm square. The wavelength coverage was from 6730 Å to 7190 Å. The slit was 1″ wide and kept in the North-South direction. It was covered with a dekker with an object and two sky apertures.

To measure linear polarization a half-wave plate is inserted into the beam. Each polarimetric measurement consists of four observations with the half-wave plate set to an angle of 0°, 22.5°, 45° and 67.5°. A calcite block located below the slit generates two beams with perpendicular polarization.

A set of polarized and unpolarized standard stars were observed during each night such that instrumental effects could be removed. The instrumental polarization was found to be $\lesssim$ 0.1 %.

The Stokes Q and U parameters were extracted in the same way as described in Paper I. In order to properly determine the emission line polarization, careful continuum subtraction is necessary. This was straightforward in spectra where the Mira variable was in its low state because then the continuum is dominated by nebular emission. In the high state (1992 observations) we also subtracted an M giant spectrum which was obtained with the same instrumentation. The λ6825 line is little affected by structure in the underlying red giant spectrum but the other Raman line lies close to the TiO absorption band at λ7088.

3. The O VI Raman features

Fig. 1 shows as an illustration the relative Stokes parameters Q/I and U/I as observed on Sep 18, 1994. The observed total flux I from all half wave plate settings is displayed in the top panel. Strong polarization signals are only visible for the Raman scattered λ6825 and λ7082 lines. We note that, as expected, both lines display a similar polarization pattern.

3.1. Continuum polarization

There is an indication of a small continuum polarization in all our observations which, within the 1 σ noise limits, seems to remain constant. Adding all observations together yields a continuum polarization of p_{con} = 0.26% at an angle of γ_{con} = 109°. (Throughout this paper we measure angles from North over East). This value is similar to the one determined in Paper I but even with the much increased continuum count rate achieved in the summed data, it remains close to the detection limit. Since this amount of interstellar polarization is expected in the area of V 1016 Cyg, we remove it from the polarization of the Raman emission lines. We note that this continuum polarization is very small and does not affect the results obtained in the following sections.

3.2. Temporal variations

Our observations in 1992 consisted of a pair of polarization measurements separated by only 18 days. Within the statistical errors there is no difference apparent on these data and we conclude that there are no short term variations. In order to improve the signal to noise ratio we have combined these two sets of data.

Figure 2 shows the intrinsic polarization in the λ6825 and λ7082 lines for our first and last observations taken in August 1991 and September 1994, respectively. The data have been corrected for the interstellar polarization and the stellar and nebular continuum radiation. We have binned the data such that in the intensity spectrum each bin had 10^6 counts for λ6825 and $2.5 \cdot 10^5$ counts for λ7082. Pure photon statistics yields errors per bin of the order of 0.1% in the percentage polarization. However, the main error source for p is the uncertainty in the continuum subtraction which becomes increasingly important in the line wings. The largest uncertainty in γ comes from the correction of the interstellar polarization and the possible but, within the limits given in the previous section, unknown presence of an intrinsic continuum polarization. Again both effects are strongest in the weak line wings. The error bars in Figure 2 represent an estimate of these uncertainties. We note that, if the continuum polarization is solely interstellar, systematic errors in the polarization angle cancel, if angle changes are measured.

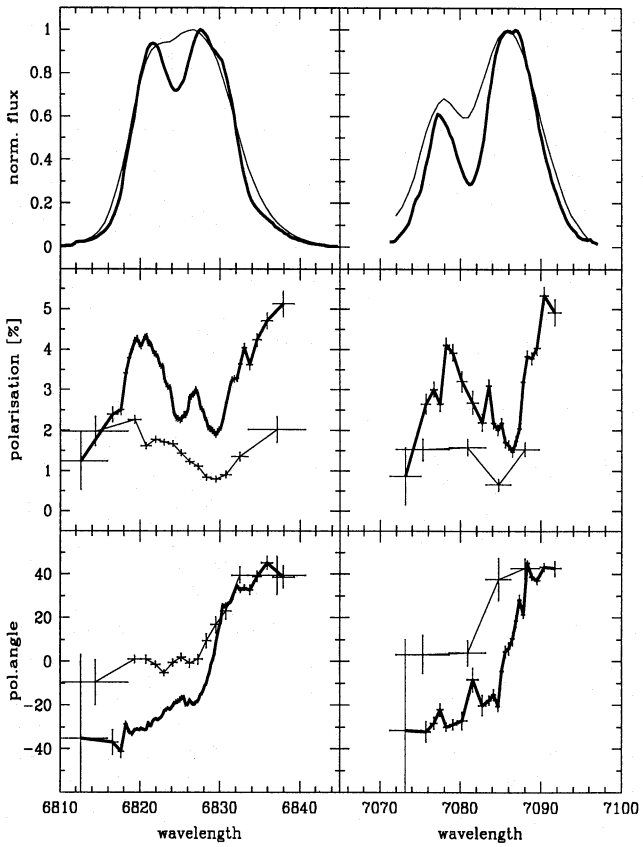

Fig. 2. Polarization structure in the Raman lines λ6825 and λ7082 for Aug 1991 (thin line) and Sep 1994 (thick line). Error bars in p and γ account for photon statistics, the uncertainty in the continuum subtraction and the interstellar correction. Note that the Aug 1991 data have an inferior spectral resolution (see text).

3.2.1. Intensity

The λ6825 and λ7082 line profiles are double-peaked, except for the August 1991 data which lacked sufficient spectral resolution. The peak-to-peak separation is about 6 Å for λ6825 and 8 Å for λ7082. The λ7082 profile differs from the λ6825 profile in that

in the former, the red peak tends to be stronger than the blue one whereas they have about the same maximum intensity in λ6825 (Fig. 2).

There is little temporal variation in the λ6825 intensity profiles with the exception of the last observation in which the red peak is stronger and extends further into the red than previously. The blue line wing does not appear to vary significantly. Also on longer time scales there is only little variation. This follows from a comparison with an échelle spectrum taken in 1982 by Stauffer (1984) which shows an almost identical Raman feature, except for a slightly less pronounced central minimum.

3.2.2. Polarization and angle

The evolution of the polarization profiles in the Raman scattered lines is summarized in Table 1 and Figs. 2 & 3. Table 1 lists the flux weighted mean percentage polarization and polarization angles for the different observations. The polarization integrated over the λ6825 line increased over the observing period by more than 50% and the angle rotated clockwise by almost 20°. This change is mainly due to the blue polarization component which is separately listed in Tab. 1. A similar time evolution is seen in the λ7082 line but the changes are less pronounced because the contribution of the "stable" red component is much stronger than for λ6825.

At roughly the wavelength of the red peak, we always see a minimum in the percentage polarization p, together with a steep gradient in the polarization angle γ (Fig. 2). The percentage polarization in the blue portion of the profile has in all (except the first) observations a clear maximum at about 2 Å shortward of the blue intensity peak. The extreme blue line wing has a significantly lower percentage polarization. In contrast, the polarization in the red line wing increases steadily towards the extreme wing, until the signal is lost in the noise. A third and new polarization bump between the central intensity minimum and the red peak appeared in the Sep 1994 observation. The details of the polarization structure described here are of interest for extracting information on the scattering geometry in V 1016 Cyg.

In Table 2 we summarize the position angle changes in the blue line wing of λ6825. To within the error bars, these changes are consistent with a constant rotation rate of 8 ± 2 °/yr. Since the blue wing of the Raman lines is produced by material which moves on or close to the binary axis towards the hot component, the observed angle changes most likely reflect aspect changes due to the binary motion.

3.2.3. Stokes Q and U

In this section we discuss the observed polarization changes in terms of the Stokes Q and U parameters. Fig. 3 shows the temporal changes of the polarization across the λ6825 profiles. Starting from the blue line wing, the polarization in each pixel increases from the 0,0 value towards the right (years 1991/92) or bottom right. As we move across the profile, the U values increase while the Q values decrease. As we finally arrive at the red end of the profile, the Q,U values return to 0. In this representation, the polarized flux $p \times I$ at a given wavelength is proportional to the length of a vector to the corresponding (Q, U) point. The increase of polarization between 1991 and 1994 is thus reflected by the considerably increased area which is enclosed by the data points. The thick lines indicate the flux weighted mean polarization on the blue side and on the red side of the central minimum. Clearly, the polarization angle rotates in the blue line wing while it stays relatively constant in the red wing. The highest polarized flux tends to occur at or near the intensity maximum of the blue peak. Particularly in the later observations we see that the polarization angle in the blue peak is well defined whereas in the red peak it spreads over a range of angles covering about one quadrant in the Q–U plane.

Table 1. Polarization parameters p and γ in the blue wing of λ6825 and integrated over the line profiles. Angles are measured North over East. Julian dates are relative to 2 440 000.

Date	JD	λ6825 total		λ6825 blue wing		λ7082 total	
		p	γ	p	γ	p	γ
Aug 1991	8 487	1.26	6.4	1.8	171	1.2	23
Sep/Oct 92	8 893	1.45	176.5	2.0	164	1.6:	177:
May 1993	9 136	1.88	172.9	2.2	160	1.6	3.8
Sep 1994	9 615	2.07	167.0	3.5	148	1.5	6.4

Table 2. Angle rotation in the blue wing of λ6825 between various observing dates.

Dates	time span [yr]	change in γ [°/yr]
Sep 1994 - Aug 1991	3.09	7.5
Sep 1994 - Sep/Oct 1992	1.98	8.0
Sep 1994 - May 1993	1.31	9.6
weighted mean		8.1 ± 2

4. Towards a binary orbit

The determination of orbital parameters from phase locked polarization changes is a well known technique in binary star research (e.g. Rudy & Kemp 1978; Brown et al. 1978; Bastien 1988, St-Louis et al. 1993 and references therein). Therefore we only briefly summarize some basic properties of light polarization from asymmetric and rotating scattering geometries. For a dipole scattering process like Raman scattering, right angle scatterings produce a large polarization while forward and backward scatterings are unpolarized. For an inclined orbit we therefore expect a polarization minimum at the conjunctions because the binary configuration is then closest to a forward or backward scattering situation. The highest polarization will

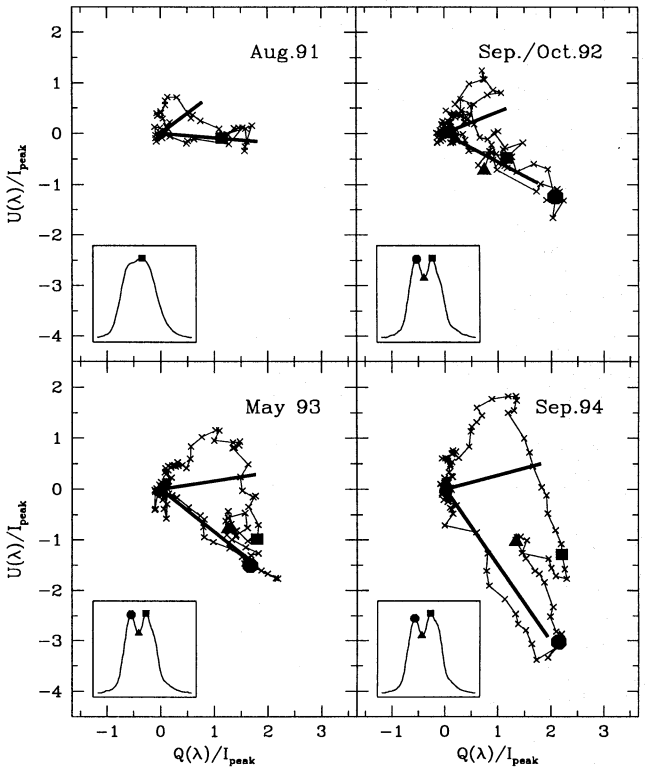

Fig. 3. Observed Stokes parameters Q versus U across the λ6825 Raman line profile at various dates. Q and U are scaled by the peak intensity $I_{\rm peak}$ and expressed as a percentage. The round, triangular and square symbols represent the blue intensity maximum, the central minimum and the red intensity maximum, respectively. The thick lines indicate the mean polarization in the blue and red line wings. The insets show the location of the filled symbols in the corresponding line profiles.

occur at quadratures when the binary configuration is optimal for right angle scatterings.

The projection of an inclined circular orbit has an effect on the observed rotation rate in the polarization angle. The angle rotation is relatively fast near conjunction and slow near quadrature. Orbits with small inclinations are always near a right angle scattering configuration. They will show a high percentage polarization with little amplitude together with steady rotation of the polarization angle.

4.1. Orbital inclination and phase

Our spectropolarimetric observations of V 1016 Cyg show a rotation of the polarization angle in the blue wing of the Raman scattered lines. In λ6825, a rotation of about 24° within three years was accompanied by an increase in the percentage polarization from 1.8% to 3.5%. The low polarization for the first observation and the rapid increase by about a factor of two indicate that we viewed the system in 1991 close to conjunction, and that it is presently moving towards quadrature. Since the polarization rate still seems to increase, we can expect that the polarization amplitude is at least twice the presently observed change of 1.7 %. The condition $p(0°) \leq 1.8\%$ for the polarization minimum at conjunction and $p(90°) \geq p(0°) + 3.4\%$ for the maximum at quadrature indicates a polarization ratio

$$R_p = \frac{p(0°)}{p(90°)} < 0.35\,.$$

According to Figure 15 of Schmid (1992) this ratio yields $i >$ 40° for the inclination of the orbital plane. The fact that we see an angle rotation at all indicates, on the other hand, that the inclination cannot be extremely large: $i \lesssim 80°$.

In summary, our spectropolarimetric observations give the following constraints on the binary orbit: an angle rotation of the binary axis of 24° in three years, an inclination in the range $i = 60° \pm 20°$ and the occurrence of the conjunction phase around Aug 1991 or shortly before. Near conjunction the binary axis was orientated East–West and hence, the line of nodes of the orbital plane has to lie roughly North–South.

4.2. Orbital period

At present, the polarimetric data is insufficient to conclusively determine the orbital period of the V 1016 Cyg system. We can however arrive at a statistical result. Using a Monte Carlo method we estimate the effects of different inclinations and orientations of polarimetrically allowed circular orbits, on the length of the orbital period. To this purpose, we draw a series of random inclinations and orbit orientations and compute the resulting orbital period by forcing the binary axis to satisfy the polarimetric observations. Taking the conditions about the inclination and the line of nodes from Sect. 4.1 into account, the distribution of orbital periods shown in Fig. 4 (full line) is obtained. Periods shorter than 55 yrs are not possible and the probability peak occurs at $\sim$ 60 yrs. The probability tail for longer periods extends to about 250 years where the distribution has a cut off. The probability for a period in the range 80 $\pm$ 25 yrs is 62 %.

There is a strong correlation between period and inclination in the sense that short periods around 60 years require $i \approx$ 40° while long periods around 250 years require $i \approx 80°$. The exact location of the nodal line has only minor effects on the distribution.

As an illustration, we also show in Fig. 4 a probability distribution with no restrictions on the inclination and the orbital phase. The previously excluded low inclination orbits $i < 40°$ create a strong probability peak for periods between 35 and 55 years. Most of the extremely short and extremely long periods are produced by orbits which have high inclinations $i \gtrsim 70°$.

4.3. Separation, kinematics and accretion

The most likely range of orbital periods from our simulations of 80 $\pm$ 25 yrs along with an assumed total system mass of 2 $M_\odot$ yields a separation between the stellar components of 23 $\pm$ 5 AU via Kepler's third law. The exact values of the system mass and period are not very important because they only enter with low exponents of 1/3 and 2/3, respectively. If the total

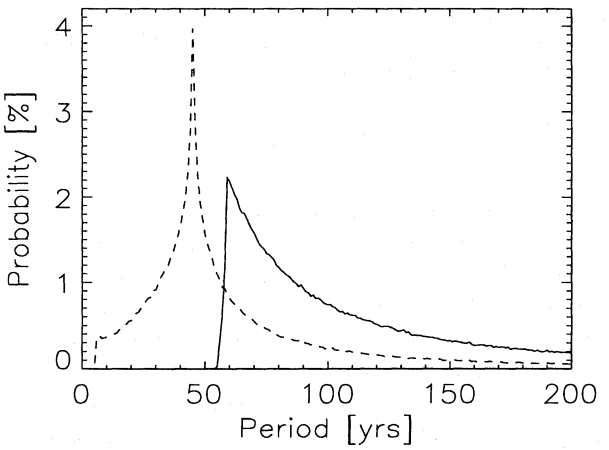

Fig. 4. Probability distribution of the periods for circular orbits which satisfy the polarimetric observations. Full line: Restriction to intermediate inclinations (see text); Dashed line: no restrictions on orbit inclination and orientation.

system mass is split into $M_{Mira} = 1.4\,M_\odot$ and $M_{comp} = 0.6\,M_\odot$, typical for the stellar components involved, the center of mass of the system would be at a distance of 7 AU from the center of the Mira. This is well beyond a typical Mira radius. The Lagrange point L_1 is at a distance of about 13.5 AU from the center of the Mira. As expected, the Mira thus clearly underfills its Roche lobe. In this orbital configuration, the velocities of the Mira and hot companion amount to about 2.5 km/s and 6 km/s, respectively. Although difficult to observe, the orbital motion of the Mira star is measurable. We note that at a distance of $\sim$ 3 kpc (Whitelock 1988) the maximum separation between the two stellar components will be about 8 mas.

We can estimate the accretion rate onto the hot companion in such a binary system. As outlined above, disk accretion through Roche lobe overflow is very unlikely. However Bondi–Hoyle accretion will occur and using the formula given in Livio and Warner (1984) we find an accretion rate of $\sim 10^{-8}$ $M_\odot$/yr. For the red giant mass loss rate and wind velocity we adopted $4 \cdot 10^{-6}$ $M_\odot$/yr and 15 km/s which are appropriate for a Mira with a 480 d period (Schild 1989, Wood 1990).

4.4. Conjunction

It is most likely that the hot component and the emission nebula were in front of the Mira during the 1991 conjunction. In the opposite case, we would expect to see variable extinction as the nebular emission has to pass through the Mira's extended neutral wind region. Observations in the far UV are extremely sensitive to the effects of dust extinction or H I Rayleigh scattering. Since 1978, V 1016 Cyg has been regularly observed with the IUE satellite and we have retrieved UV spectra covering 14 years up to 1992 from the archive. We found that during this period there are no indications for a variable dust extinction e.g. in the line ratios of [Ne V] λ1575/λ2973 or He II λ1640/λ3203. There is also no sign of a variable H I Rayleigh scattering column density e.g. in the N V λ1240 line flux. The effect of Rayleigh scattering on the N V light curve is simulated in Schmid (1995). According to these models (e.g. SB3) we can exclude a phase angle $\alpha > 135°$ for the entire IUE era. In these models α is the angle between the binary axis and the line of sight, where $\alpha = 180°$ means that the Mira is in front of the hot component. Thus, a conjunction with the Mira in front of the emission nebula would have been detected in the IUE data even if the orbital inclination were as low as 40°. We therefore conclude that the hot component and the emission nebula was in front of the cool giant during the recent conjunction.

5. Scattering geometry and circumstellar environment

The polarimetric profiles of the Raman scattered lines in V 1016 Cyg show a complex wavelength dependence. They can however provide interesting information on the matter distribution in the inner binary system. In the following discussion we apply to the Raman lines the basic ideas of the scattering model outlined in Paper I.

We assume that the O VI photons are initially released in the ionized region near the hot component. These O VI photons may then penetrate into the neutral wind of the cool giant and convert in a Raman scattering process to λ6825 or λ7082 photons. The scatterings produce polarized light with a polarization angle perpendicular to the direction of the incoming photons. A special feature of the O VI Raman scattering process is that it multiplies the Doppler shifts produced by the motion of the scattering H^0-atoms relative to the direction of the incoming photon by a factor of about 6.7 (Schmid 1989). As a result we expect that the photons in the blue line wing received a Doppler shift by approaching H^0-scatterers with respect to the O VI source while the red line wing photons are scattered by receding H^0-atoms in the red giant's wind (see Paper I for details).

The Raman lines in V 1016 Cyg show a steady counterclock wise rotation in the polarization angle γ from the line center to the red line wing. We note that this wavelength dependent rotation is a clear sign that the scattering geometry has no rotational symmetry around the binary axis. In Paper I we showed how geometric compensation in a rotationally symmetric system produces polarization with only two polarization angles perpendicular to each other. Thus we have to abandon rotational symmetry for the scattering geometry and invoke a 3-dimensional model for V 1016 Cyg. The orbital motion is a likely cause for producing ionization structures and H^0-density distributions which deviate from rotational symmetry.

5.1. A 3-dimensional model

We use as a guide the explorative 3D-hydrodynamical calculations by Walder (1993) for the symbiotic binary system EG And. They simulated the interaction between a fast stellar wind from the hot component and a much denser, slow wind from the cool component in a rotating binary system. The resulting interaction zone has the shape of a warped surface which lags behind the corresponding structures of a rigidly rotating sys-

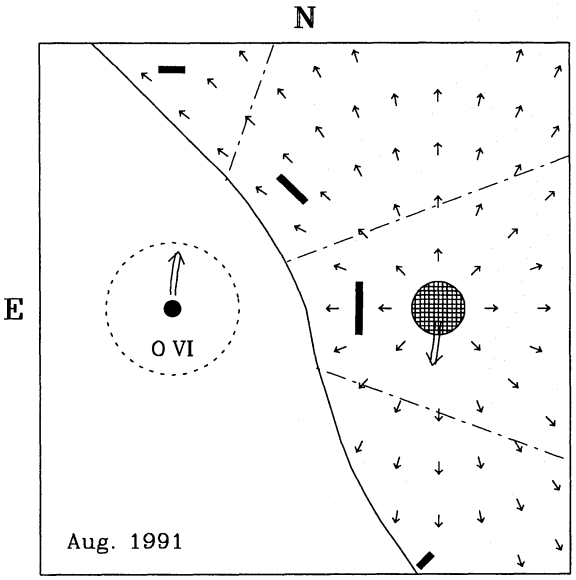

Fig. 5. Sketch of the inner V 1016 system. The dashed line shows the O VI emission line region around the hot component. Raman scatterings occur in the spherically symmetric neutral Mira wind (small arrows) which is separated from the ionized region by the ionization front (full line). The thick lines indicate the expected polarization angle and scattering intensity (length) of the Raman scattered O VI lines from different cone shaped regions (dashed dotted lines). The orbital motion is indicated by double arrows.

tem. Figure 5 is a simplified sketch of the innermost region of Walder's model, which we will adopt here for V 1016 Cyg. The interaction zone coincides with a large density step that divides the dense red giant wind from the tenuous, fast wind from the hot component. Due to the density step, we may assume that the ionization front also follows this pattern. Thus, the important features of our model for the Raman scattering problem are that the Mira variable has a radially symmetric neutral outflow which is terminated on the hot component's side by a warped ionization front and that an O VI source is located around the hot component (Fig. 5).

In August 1991, the orientation on the sky of the binary axis was East-West. In Fig. 5 we have plotted the hot component East of the cool component. In principle, it could also be on the other side, as spatially unresolved spectropolarimetric data are invariant to a rotation by 180° of the scattering geometry. Between Aug 1991 and Sep 1994 the binary rotated clockwise by about 24° as inferred from the rotation of the polarization angle in the blue line wing. This binary rotation of the stellar components is indicated in Fig. 5 by the two double arrows.

Such a configuration for V 1016 Cyg can now give a plausible explanation for the wavelength dependence of the polarization angle in the Raman scattered O VI lines. As outlined above, the blue line wings of the Raman scattered lines consist mainly of photons which obtained a Doppler shift by H^0-scatterers that are approaching the O VI photon source. For a spherically symmetric Mira wind these photons must be produced in that part which faces and moves towards the hot component. This scattering region is relatively small and the incoming photons have a well defined general flight direction along the axis connecting the two binary components. The resulting polarization is therefore relatively strong and the polarization angle is perpendicular to the binary axis.

The red line wing is mainly due to Raman photons from a scattering process with receding H^0-atoms. Different and extended regions in the Mira wind have such a velocity with respect to the O VI photon source. However, in our model, it is expected that the dominant contribution to the red line wing comes from the region or the cone NW from the hot component in Fig. 5, producing a light polarization with an angle of about 45°. This region is strongly irradiated by the O VI line source because the geometric dilution is small and the H^0 density in the giant's wind is still relatively high, factors which favour the Raman process. The cone SW of the hot source partially compensates the NW component and reduces the percentage polarization in the 45° polarization component. However, the asymmetric shape of the ionization front significantly favours the scattering contribution of the NW cone.

The exact polarimetric structure in the Raman lines is determined by a complex interplay between geometric compensation, photon escape probability and multiple scattering effects in and between the different scattering regions. These effects should, however, not affect the general features of the resulting spectropolarimetric structure of the Raman lines.

Thus, our model qualitatively explains the main features of the observed polarization profile. The model associates the more strongly polarized blue line wing with a position angle of about 0° and a red line wing with a position angle of about 45° with different scattering regions in the Mira wind. We further expect that the blue polarization component shows a more "rigid" rotation with the orbital motion than the red component which originates from scatterings further out in the giants' wind in a more fluffy region. Additionally, our model links the shape of the scattering region with the orbital motion which produces the lagging front dividing the ionized and neutral region. As a result, we see in the Raman line a wavelength dependent rotation in the polarization angle from the blue to the red line wing that is opposite to the time dependent and phase locked rotation of the polarization angle of the entire line.

5.2. Interpreting other observations of V 1016 Cyg

The outer nebular structure of V 1016 Cyg is revealed by a radio map taken with the VLA at 1.3cm in December 1980 (see Hjellming & Bignell 1982; Taylor 1988). The map shows two emission peaks separated by about 0.1″ in a NE–SW direction which are embedded in a larger (0.3 – 0.5″) low surface brightness region with an E–W elongation.

From our spectropolarimetric orbit we can estimate the orientation of the binary axis for the 1980 VLA radio map. Assuming that the conjunction occurred in Aug 1991 and an inclination between 40° and 80° gives, for the measured rotation of about 8° ± 2°, a position angle of the binary axis between 125° and 155° for the 1980 epoch. The two main emission peaks in the

1980 radio map were thus orientated roughly perpendicular to the binary axis. This may be an accidental coincidence but there could also be a tight relationship between the innermost radio structure and the binary axis.

Interesting observations on the subarcsecond structure of V 1016 Cyg were also reported by Solf (1983,1988). With high resolution spectroscopy he found two emission components in the [N II] λ6584 line and the green [O III] lines. The two components in [N II] are separated by 0.4 arcsec in space and by 51 km/s in radial velocity. The position angle of the two lobes is about 80° and roughly coincides with the outer, low surface brightness region of the 1.3cm VLA map. The East component has a receding velocity while the West component is approaching us. The [O III] lines show the same qualitative behaviour but with a smaller spatial separation. Solf (1983) interprets his data as a bipolar outflow perpendicular to the orbital plane. Our spectropolarimetrically derived orbit supports this interpretation. We find that the binary axis has roughly an East–West orientation for the conjunction phase. Thus, the line of nodes for the orbital plane is roughly North–South which is, as predicted by Solf, perpendicular to the bipolar outflow. From Solf's outflow model we can eliminate the 180°-ambiguity in our spectropolarimetric orbit. The fact that the polar outflow heading East is receding implies that the orbital plane is inclined Eastward, so that the hot star was in front and East of the cool component during the 1991 conjunction (as in Fig. 5).

6. Raman scattered C II $\lambda\lambda$7023,7054 lines

In symbiotic systems, Raman scattering at neutral hydrogen is not only expected to act on the O VI $\lambda\lambda$1032,1038 photons. Other far UV emission lines with wavelengths near the H I Lyβ, Lyγ, etc. transitions may equally produce broadened Raman features in the visual wavelength region (see Nussbaumer et al. 1989). Such features have been detected in the spectrum of RR Tel at λ4851, λ4332.6 and λ4977.0, and were attributed to Raman scattered He II λ972.1, He II λ949.3 and C III λ977.0, respectively (van Groningen 1993).

Our WHT observations of V 1016 Cyg provide evidence for additional Raman scattered lines. The intensity spectra of May 28, 1993 and Sep 18, 1994 show two weak, broad emission features at λ7021 and λ7052. The same spectroscopic signature can also be recognized in the high resolution spectrum of the symbiotic system RR Tel plotted in Schild & Schmid (1992). We suggest that these features are due to Raman scattering of the C II ^{2}P°$-^2$S doublet $\lambda\lambda$1036,1037 by neutral hydrogen.

Fig. 6 shows the features in the September 1994 spectrum. Terrestrial absorption lines have been removed with a spectrum of the B0 V star HD 204827 (polarimetric standard star). The C II Raman lines are only seen in spectra taken near the light minimum of the Mira variable. Near light maximum (1992 observations) strong absorption structures from the Mira are superposed and the two C II Raman lines are hardly visible.

Taking for the C II vacuum wavelengths 1036.332 Å and 1037.014 Å respectively, and using 82258.95 cm^{-1} for the energy of the final hydrogen state 2^2S, the expected air wavelengths for the Raman lines are 7022.75 Å and 7054.18 Å. This agrees well with the measured central rest wavelengths of the observed features, which are at 7022.9 ± 0.7 Å and 7054 ± 2 Å. The relatively large errors, especially for the λ7054 component, account for the uncertainties caused by blending with other nebular emission lines.

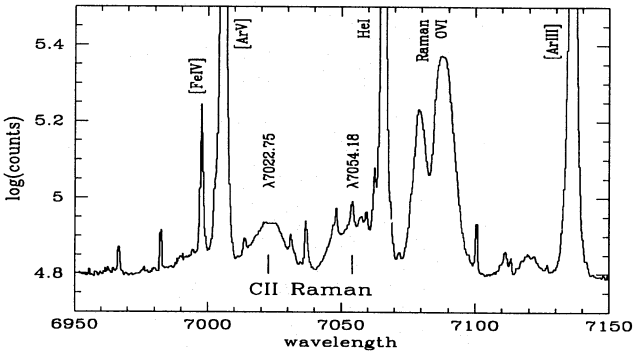

Fig. 6. C II Raman features in the spectrum of V 1016 Cyg obtained in September 1994.

The full width at half maximum (FWHM) of the λ7023 component is about 12.5 ± 2.5 Å. The λ7054 component has probably the same width but severe blending prevents a reasonable measurement. According to the line profile study of Kindl et al. (1982) a FWHM of about 0.10±0.05 Å is expected for the C II $\lambda\lambda$1036,1037 lines in V 1016 Cyg. This corresponds to a velocity dispersion for the emitting C^+ ions of ±15 km/s. With the same velocity dispersion for the scattering H^0 atoms, the multiplication of relative line widths in the scattering process (factor 6.8) gives a width of about 9.2 Å for the C II Raman lines. This value is marginally lower than the measured line widths but still in reasonable agreement if we consider the uncertainties in the widths of the far UV C II lines or possible additional Doppler shifts due to multiple scatterings or turbulent gas motions.

The C II lines λ1036 and λ1037 have the same upper level and an emissivity ratio of $\Lambda_{UV} = F(\lambda1036)/F(\lambda1037) = 0.5$ is expected under optically thin (nebular) conditions. However, we expect a C II line ratio $\Lambda_{UV} \approx 1$ in V 1016 Cyg, because the nebular densities are so high that self–absorption is important. A similar effect is observed for the O I λ1305 multiplet (Nussbaumer & Schild 1981). The two features λ7023 and λ7054 have roughly the same strength. Raman scattering does not significantly change the intensity ratio because of the small wavelength separation. Thus, the relative strengths of the λ7023 and λ7054 lines reflect the UV C II emission line ratio.

We conclude that the wavelengths, line widths and intensities support the proposed identification of the λ7023 and λ7054 features as Raman scattered C II $\lambda\lambda$1036,1037 lines. The UV C II lines are expected to be emitted near the interface between the ionized nebula and the neutral wind of the cool giant, i.e. in a region where a substantial fraction of hydrogen is neutral and therefore C II Raman scattering is facilitated. The geometry for C II Raman scattering is less well defined than for O VI and we expect only a small net polarization in the λ7023 and λ7054

features. In addition, the weakness of the scattered lines will make a polarization measurement very difficult.

7. Discussion

7.1. Orbital parameters

To measure the orbital periods of symbiotic Miras is a difficult task which demands patience and long lasting research funds. Methods used in the past dealt with looking for periodic changes in e.g the emission line spectrum or extinction variations. So far, the results have been inconclusive or were subsequently shown to be wrong. Dust obscurations have been detected in several symbiotic Miras (Willson et al. 1981, Feast et al. 1983, Whitelock et al. 1983, Whitelock 1987). If these obscurations are indeed orbitally–related, then future IR observations can, in principle, provide the binary periods.

Here we illustrate how changes in the polarization of the Raman scattered emission lines can be used to derive information about symbiotic binary orbits. In the case of V 1016 Cyg, we observed a clockwise rotation of the polarization angle in the blue line wing of λ6825 of 8°/yr over a period of 3 years. During the same period the total line polarization increased from 1.3% to 2.1%, i.e. by 0.26%/yr. We can interpret this increase in terms of orbital motion. The low polarization observed in Aug 1991 indicates that the system was close to a backscattering configuration and therefore close to conjunction. The marked increase implies an intermediate or high inclination. The fact that we see an angle rotation at all shows, on the other hand, that the inclination cannot be very high. We consider as the most likely inclination $i = 60° \pm 20°$. The period probability distribution for polarimetrically allowed, circular orbits has a maximum around 60 yrs and we expect the period to lie in the range 80±25 yrs.

Our spectropolarimetrically determined orientation of the orbital plane provides interesting complementary information to previous, spatially resolved observations. In particular the bipolar outflow model of Solf (1983) is strongly supported.

At present, we do not have enough data to determine a more accurate orbital period and inclination. Only further observations spread over a period of many years will achieve this. As the V 1016 Cyg system moves on from conjunction towards quadrature we expect the polarization to further increase in the coming decade and reach values of 10% or even more. We see the data presented in this paper only as a first step, which in conjunction with later polarimetric measurements carried out by perhaps even a future generation of observers, will ultimately lead to accurate orbital parameters.

7.2. Geometry of the V 1016 Cyg system

Polarization measurements of Raman scattered O VI emission lines by neutral hydrogen are a powerful tool to investigate the 3-dimensional structure of symbiotic systems. We found from the wavelength dependent rotation in the polarization angle that the scattering geometry in V 1016 Cyg as projected on the sky has no mirror symmetry. Geometric compensation of the polarization signal in a configuration with mirror symmetry would produce a polarization profile having either one fixed polarization angle or a flipping angle between two components which have to be perpendicular. We therefore have to abandon a rotationally symmetric geometry for V 1016 Cyg, because any such scattering configuration has a mirror symmetry when projected on the sky.

We adopt a neutral matter distribution which is inspired by hydrodynamical calculations by Walder (1993) that include the effects of the orbital motion. This model is characterized by a warped ionization front which lags back compared to the "rigid" rotation case. This model can qualitatively explain the observed polarization properties. We should emphasize that such a warped matter distribution may not only be required for V 1016 Cyg but also for other symbiotic systems. At least 4 out of 15 objects (Z And, V 1016 Cyg, He2-106 and AS 316) in the polarimetric survey in Paper I must have scattering structures which strongly deviate from a mirror symmetry.

Acknowledgements. We are indebted to the La Palma support astronomers who carried out the service observations. We are particularly indebted to René Rutten and Vik Dhillon. It is a pleasure to thank Stephen N. Shore, U. Mürset and H. Nussbaumer for useful comments on the manuscript. This work was financially supported by the Swiss National Science Foundation.

References

Anandarao B.G., Sahu K.C., Desai J.N., 1985, Ap&SS 114, 351
Bastien P., 1988, in: Polarized Radiation of Circumstellar Origin, Coyne et al.(eds.), Vatican Observatory, p. 595
Brown J.C., McLean I.S., Emslie A.G., 1978, A&A 68, 415
Corradi R.L.M., Schwarz H.E., 1993, A&A 268, 714
Eyres S.P.S., Kenny H.T., Cohen R.J., Lloyd H.M., Dougherty S.M., Davis R.J., Bode M.F., 1995, MNRAS 274, 317
Feast M.W., Catchpole R.M., Whitelock P.A., Carter B.S., Roberts G., 1983, MNRAS 203, 373
Girard T., Willson L.A., 1987, A&A 183, 247
Hack W.J., Paresce F., 1993, PASP 105, 1273
Hjellming R.M., Bignell R.C., 1982, Science 216, 1279
Kindl C., Marxer N., Nussbaumer H., 1982, A&A 116, 265
Livio M., Warner B., 1984, The Observatory 104, 152
Merrill P.W, 1950, ApJ 112, 514
Munari U., 1988, A&A 200, L13
Nussbaumer H., Schild H., 1981, A&A 101, 118
Nussbaumer H., Schmid H.M., 1988, A&A 192, L10
Nussbaumer H., Schmid H.M., Vogel M., 1989, A&A 211, L27
Nussbaumer H., Walder R., 1993, A&A 278, 209
Paresce F., Hack W., 1994, A&A 287, 154
Rudy R.J., Kemp J.C., 1978, ApJ 221, 200
Schild H., 1989, MNRAS 240, 63
Schild H., Schmid H.M., 1992, Gemini - Newsletter RGO 37, 4; reprinted in Current Science 63, 536
Schmid H.M., 1989, A&A 211, L31
Schmid H.M., 1992, A&A 254, 224
Schmid H.M., 1995, MNRAS 275, 227
Schmid H.M., Schild H., 1990, A&A 236, L13
Schmid H.M., Schild H., 1994, A&A 281, 145 (Paper I)
Schwarz H.E., Aspin C., Lutz J.H., 1989, ApJ 344, L29
Solf J., 1983, ApJ 266, L113

Solf J., 1988, in: The Symbiotic Phenomenon, IAU Coll. 103, eds. J. Mikolajewska et al., Kluwer, p. 85
Solf J., Ulrich H., 1985, A&A 148, 274
Stauffer J.R., 1984, ApJ 280, 695
St-Louis N., Moffat A.F.J., Lapointe L., et al., 1993, ApJ 410, 342
Taylor A.R., 1988, in: The Symbiotic Phenomenon, IAU Coll. 103, eds. J. Mikolajewska et al., Kluwer, p. 77
van Groningen E., 1993, MNRAS 264, 975
Walder R., 1993, Thesis ETH Zürich No. 10302
Wallerstein G., 1986, PASP 98, 118
Wallerstein G., Willson L.A., Salzer J., Brugel E., 1984, A&A 133, 137
Whitelock P.A., 1987, PASP 99, 573
Whitelock P.A., 1988, in: The Symbiotic Phenomenon, IAU Coll. 103, eds. J. Mikolajewska et al., Kluwer, p. 47
Whitelock P.A., Feast M.W., Catchpole R.M., Carter B.S., Roberts G., 1983, MNRAS 203, 351
Willson L.A., Garnavich P., Mattei J.A., 1981, Inf. Bull. Var. Stars, No. 1961
Wood P.R., 1990, in "From Miras to Planetary Nebulae: Which Path to Stellar Evolution ?", eds. M.O. Menessier & A. Omont (Yvette Cedex: Editions Frontières), p. 67

This article was processed by the author using Springer-Verlag LaTeX A&A style file version 3.